Experimental determination and simulations of the Huynen target parameters for full polarimetric millimetre wave concealed weapon recognition

Eddie Blackhurst[a], Neil Salmon[b], Matthew Southgate[b], [a]School of Physics and Astronomy, The University of Manchester, Jodrell Bank, SK11 9DL. [b]Faculty of Science and Engineering, Manchester Metropolitan University, All Saints, Oxford Road, M15 6BH.

ABSTRACT

The Huynen polarisation fork as a representation of the full polarimetric radar signature represents a unique and natural description of a target. This paper investigates the use of full polarimetric radar operating over the band 18-26 GHz to measure the Huynen target parameters of size, orientation, helicity, skip angle and fork angle from a range of canonical polarimetric radar targets and classic concealed weapon surrogates. Measurement will determine how accurately the Huynen target parameters represent the geometries of the canonical targets and surrogate weapons such as concealed metal and ceramic guns, shrapnel and plane sheet dielectrics. Target backgrounds will be large area absorbers and the human body to enable assessment of the capability for stand-off concealed weapons detection. The system used for the measurement comprises a dual channel vector network analyser, a Turnstile orthomode transducer (OMT) and a conical horn antenna. The OMT has an isolation better than -35 dB between orthogonal polarisations. This system measures and calibrates the Sinclair matrices of targets, from which the Huynen target parameters are derived. A simple model of targets based on the original work in Huynen thesis back in 1970 will be presented, enabling comparison between measured and simulated Huynen target parameters to be made. Conclusions are that experimental measurements of the Huynen target parameters of canonical and surrogate targets agree well with the basic theory of the technique and simple model simulations.

Keywords: Concealed weapons detection, FMCW radar, Mono-static radar, full polarimetry, millimetre wave radar, non-imaging sensor, Radar calibration, Huynen polarization fork.

1. INTRODUCTION

This work continues the investigation into coherent full polarimetric radar techniques to maximise acquired information content from scenarios where spatial information content is fundamentally limited due to the effects of effects [1]. In a stand-off security screening scenario millimetre wave techniques have the advantage of being able to penetrate clothing and potential to detect concealed weapons such as person born improvised explosive devices (PBIED) and knives both of metallic or ceramic construction [2], [3], [4], [5], [6], [7]. Target detection using circular polarisation has been trialled [8] and full polarimetry for security screening was initially investigated in [9], [10] using a pseudo monostatic (transmitter and receiver co-located). This used adjacent transmitter and receiver antennas and ran a number of decomposition algorithms on experimental data [11]. The work presented here is truly monostatic utilising one corrugated conical horn antenna for transmit and receive. Horizontal and vertical polarisation is generated with use of a linear polariser.

The aim of this paper is to apply the Huynen Polarisation fork and parameter analysis approach to as set of classical canonical radar targets such as plane, dihedral, and dipole structures as well as for a wax block. Comparison of measured results with theoretical will be made. Huynen polarisation parameters and associated fork represent the targets physical characteristics, based on the location of the co and cross polar nulls [12]. The paper demonstrates that the Huynen target size parameter can be used to ascertain thickness of dielectric targets and that the orientation angle of objects such as dipole features can be determined. Radar measurements have been taken in a laboratory environment with utilisation of a background of radar absorbent material (RAM) and a working range of two meters. The measurements presented are for the coherent case where the target and measurement equipment are static and hence no depolarisation is present.

Understanding the signatures of classical canonical radar targets should then enable the technique to be refined and extended to longer range.

2. METHOD

The radar presented in this paper is of the monostatic non-imaging type, based around Sinclair matrices generated from measurements made using a Keysite PNAX VNA, with a swept frequency range covering 18 to 26 GHz (K-band). The radar is of the frequency modulated continuous wave (FMCW) type. Figure 1 shows a block diagram of the radar, indicating the key elements: the VNA, the orthomode transducer (OMT) and the corrugate conical horn antenna. The OMT is of the linear polariser turnstile type and is of 'split block' construction with isolation of better than -35 dB between orthogonal polarisations [13], [14].

The system exploits the two ports of the VNA to send out and measure separately the return from two coherent waves. The OMT is arranged to combine orthogonally these two waves in a single waveguide, so that one becomes the horizontal polarisation and the other the vertical linear polarisation. The system thus constitutes a true monostatic measurement system, set to measure in the orthogonal linear polarisation basis. This enables horizontal polarisation to be transmitted to the target and simultaneous measurements to be made on both the horizontal and vertically polarised returns. The VNA calculates the S-parameters in the standard way, so with the OMT on the frontend, these parameters constitute directly the elements of the Sinclair back scatter matrix (Eq 1). The VNA based radar provides both magnitude and phase information for the co and cross polar responses produced by the targets. Table 1 shows the radar's specification.

$$S = \begin{bmatrix} S_{11} & S_{12} \\ S_{21} & S_{22} \end{bmatrix} = \begin{bmatrix} S_{HH} & S_{HV} \\ S_{VH} & S_{VV} \end{bmatrix} \quad (1)$$

In the monostatic configuration the Sinclair matrix is complex symmetric, so contains only three different complex numbers.

Calibration is carried out in two stages, the first by calibrating the VNA up to the end of the test leads with waveguide to coax transitions fitted utilising the standard through, reflect, line (TRL) approach. The second level of calibration carried out is used to minimise the effects of any differences in path length in the OMT and horn assembly as well as any stray cross polarisation that may be present [15], [1]. This is done via the carful measurement of a set of calibration targets comprising a flat plate, dihedral orientated at 45° between orthogonal polarisations and a wall of radar absorbent material (RAM). The flat plate, dihedral and any other targets measured have their responses subtracted from the measured background of RAM (Eq 2) this helps to remove any unwanted reflections that the OMT and horn might have. All measurements are made in the frequency domain.

$$Calibrated\ Target = \frac{(Target - RAM)}{(DH45° - RAM) + (Plate - RAM)} \quad (2)$$

Sinclair matrices in the frequency domain are transformed once calibration has been performed in to the time domain via the application of an Inverse Fast Fourier Transform (IFFT) so gating can be used to remove clutter from surrounding objects in the laboratory. A rectangular window is applied to the measured calibrated target data to remove the small amount of clutter present in the measurement range. The target position was fixed at a range of 2.1 meters, the gate open at a range of 2 meters and closed again at a range of 2.3 meters. Conversion back to the frequency domain is then applied as all further data processing is done in the frequency domain.

Table 1. FMCW Radar specification.

Frequency Range	18 to 26 GHz		Sweep time	98.859mS
Number of points	801		I.F. bandwidth	10 KHz
Number of samples per point	10		Antenna gain	20 dBi
Maximum usable range	15 meters		3dB beamwidth	13°
Range resolution	1.875 cm			

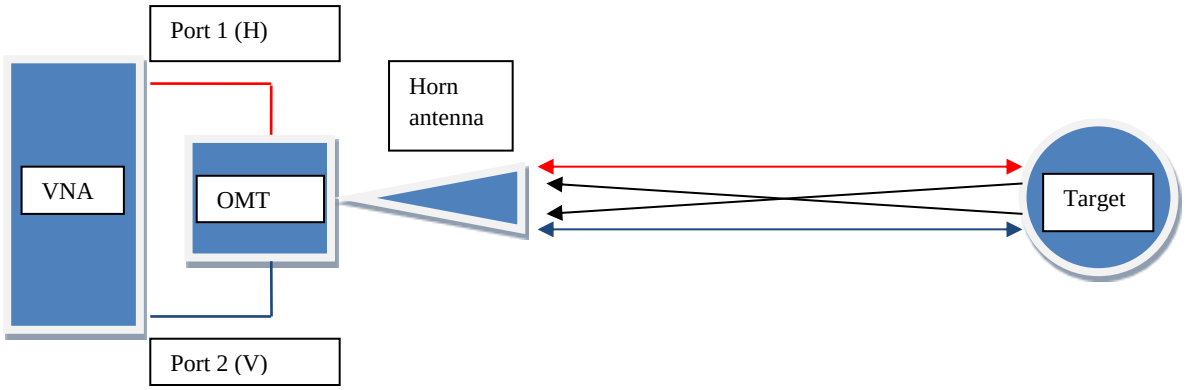

Figure 1. A schematic of the full polarimetric monostatic FMCW radar

3. POLARISATION ON THE POINCARÉ SPHERE

Graphical representation of any polarization state can be defined as a point P when plotted on the Poincaré sphere (Figure 2a) [16]. This unit radius sphere was developed by Poincaré in 1892 to represent the polarization states of polarized light. The zenith represents left hand circular (LHC) and the nadir right hand circular (RHC) polarisation. All of the linear polarisation states lie around the equator. Elliptical polarisation states lie everywhere else. Two angles are required to define the point P on the sphere, (τ, ϕ) or (α, δ), the latter two being referred to as the Deschamps (or spinor) and their values range accordingly:

- τ: Ellipticity angle ($-\pi/4$ to $+\pi/4$), $-\pi/4$ (LHC), 0 (linear), $+\pi/4$ (RHC).
- ϕ: Orientation (tilt) angle ($-\pi/2$ to $+\pi/2$), (τ, ϕ)
- α: Auxiliary (or spinor) angle (0 to $+\pi/2$)
- δ: Phase difference ($-\pi$ to $+\pi$) between two orthogonal linear polarisations

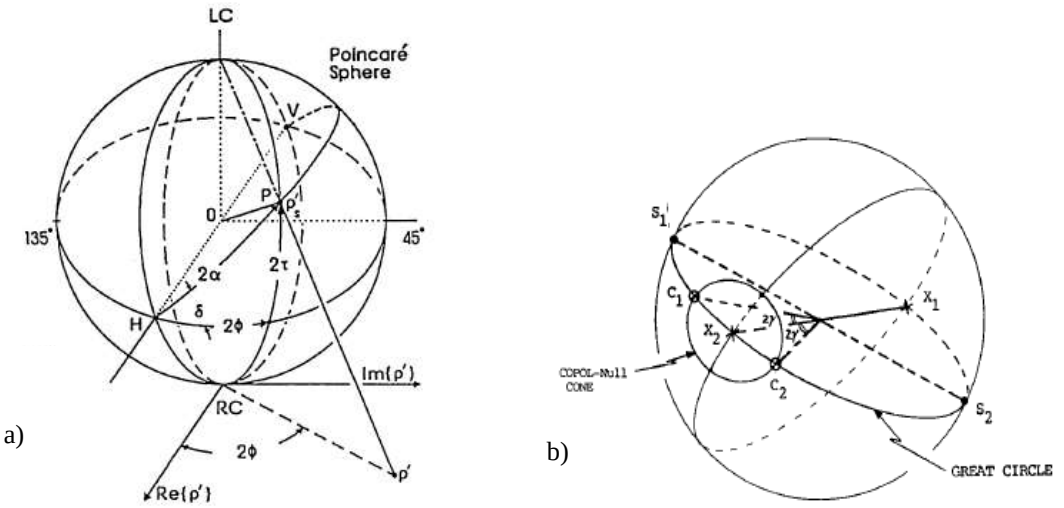

Figure 2a. Polarisation state on Poincaré sphere. [16] Figure 2b. Polarisation fork on Poincaré sphere. [17]

4. THE HUYNEN-FORK POLARISATION PARAMETERS

The Huynen polarisation fork developed on early work carried out on minimum-maximum polarisation state analysis was initially developed by Kennaugh [18] and further developed by Huynen [19]. The Huynen polarisation fork represents the monostatic, reciprocal (symmetric matrix) case, with all of the six characteristic polarization states lying on a great circle on the Poincaré sphere. The fork when plotted on the Poincaré sphere has one handle and three prongs (Figure 2b), with two additional antipodal (X-pol max) points at right angles to the handle. In total there are three distinct pairs of characteristic polarisation states (on the Poincaré sphere) for a monostatic radar:

- X-pol null (X1) and the Co-pol max are co-located (the handle)
- X-pol null (X2) – a second one is exactly opposite of X1
- Co-poll nulls(C1, C2) (symmetric about X2-origin at an angle of 2γ from X2)
- X-pol max's (S1, S2) (antipodal and at 90° from X2)

The cross polar nulls are the same as the co-polar maximums and are always antipodal (at 180°, opposite) to one another when plotted on the Poincaré sphere. The cross polar maxima and saddle points are distinct and also antipodal. The co-polar nulls are in the same plane on the Poincaré sphere as the cross polar null\co-polar maximum pair [20] . Cross polar null X1 forms the handle connected with X2 which forms the central prong of the fork, with the co-polar nulls forming the other two prongs either side, all on the same plane in the Poincaré sphere. Figure 2b [17] shows an example of the fork represented on the Poincaré sphere. The Huynen target parameters [19] are composed of seven fundamental parameters (listed below) which are generated from the three complex numbers of the Sinclair matrix. The Huynen polarisation parameters are derived from the cross polar nulls (ρ-formulation) [16].

There are seven Huynen geometrical target parameters;

1. m = Target size.
2. ϕ_m = Target orientation (tilt) angle. ϕ (-π/2 to +π/2) about the view direction in the horizontal plane of the Poincaré sphere.
3. τ_m = Target Ellipticity angle: the angle of the Copol max and Xpol null (X1) on the Poincaré sphere, ranging from -π/4 to +π/4. Some refer to this as the target helicity and it is zero for symmetric targets.
4. ν = Target skip angle: ν (-π/4 to +π/4) 0 for flat plate, π/4 radians for dihedral, π/8 radians for quarter waveplate and is related to the number of reflections from the target.
5. ϒ = Target characteristic (fork) angle, varying 0 to π/4.
6. δ_m = Phase of the polarisation ratio of the co-polar maximum varying from -π to +π.
7. α_m = Spinor angle, varying from 0 to +π/2.

that are generated from just three parameters; ρ_{xn1} or ρ_{xn2} and λ_1 and λ_2

Cross Polar Null's in HV basis are given by:

$$\rho_{xn1,2} = \frac{-B \pm \sqrt{(B^2 - 4AC)}}{2A} \tag{3}$$

$$A = S_{HH}{}^* S_{HV} + S_{HV}{}^* S_{VV} \tag{4}$$

$$B = |S_{HH}|^2 - |S_{VV}|^2 \tag{5}$$

$$C = -A^* \tag{6}$$

Co Polar Null's in HV basis are given by:

$$\rho_{cn1,2} = \frac{(-S_{HV} \pm \sqrt{(S_{HV}^2 - S_{HH}S_{VV})})}{S_{VV}} \tag{7}$$

The co and cross polar nulls presented in this paper are calculated in the linear (HV) basis but could easily be defined in another basis via the simple application of a unitary transformation.

Deschamps parameters for the co and cross polar nulls are:

$$\alpha_{n1,2} = \tan^{-1}(|\rho_{n1,2}|) \tag{8}$$

$$\delta_{n1,2} = \arg(\rho_{n1,2})) \tag{9}$$

Phase of the unitary transformation matrix [U] ψ_1 and ψ_4 are:

$$\psi_1 = -\frac{\delta_{xn2}}{2} - \frac{\pi}{2} \tag{10}$$

$$\psi_4 = \frac{\delta_{xn2}}{2} - \frac{\pi}{2} \tag{11}$$

Orientation angle ϕ for the co and cross polar nulls are:

$$2\phi_{n1,2} = \tan^{-1}(\tan 2\alpha_{n1,2} \sin \delta_{n1,2}) \tag{12}$$

Ellipticity angles of co and cross polar nulls are:

$$2\tau_{1,2} = \sin^{-1}[\sin(\delta_{n1,2}) \sin(2\alpha_{n1,2})] \tag{13}$$

Unitary transformation matrix is:

$$[\mathrm{U}(\rho_{xn1})] = \frac{1}{\sqrt{(1+\rho_{xn1}\rho_{xn1}{}^{*})}} \begin{bmatrix} 1 & j\rho_{xn1}{}^{*} \\ \rho_{xn1} & -j \end{bmatrix} \tag{14}$$

Transformation of the Sinclair matrix in the new basis is:

$$[S'(AB)] = [U(\rho_{xn1})]^T [S][U(\rho_{xn1})] \tag{15}$$

Basis vector based on ρ_{xn1} of the Sinclair (HV) matrix gives;

$$[S'(AB)] = \begin{bmatrix} \lambda_{11} & 0 \\ 0 & \lambda_{22} \end{bmatrix} \tag{16}$$

Target characteristic (fork) angle Υ is:

$$\Upsilon = \frac{1}{2}\tan^{-1}\sqrt{\frac{|\lambda_{22}|}{|\lambda_{11}|}} \tag{17}$$

Target skip angle ν is:

$$\nu = \frac{1}{4}(\arg(\lambda_{11}) - \arg(\lambda_{22})) \tag{18}$$

Target size *m* is:

$$m = |\lambda_{11}| \tag{19}$$

Target spinor parameter α_m is:

$$\alpha_m = \tan^{-1}|\rho_{xn1}| \tag{20}$$

5. RESULTS

Plots of the Huynen polarisation fork are presented in this paper via measurement and compared to theoretical for the targets listed below. Table 2 provides details of physical target dimensions for reference. The results presented are plotted on the Poincaré sphere a descriptive representation of which can be seen in Figure 2. For the measured results the cross polar null X2 is represented by blue (X)'s, the X1 nulls are represented by red (+)'s, the co-polar nulls (C1 and C2) are shown as (O)'s for the measured responses presented below.

1. Flat metal plate. (Figure 3 left).
2. Dihedral reflector angled at 45° between orthogonal polarisations. (Figure 3 right).
3. Vertical and horizontal dipoles. (Figure 4 left and right).
4. Wax block. (Figure 9 left).

Table 2. Target physical dimensions.

Target type	**Length(cm)**	**Width(cm)**	**Details**
Flat plate	87	64	
Dihedral	50	50 (aperture)	2 sides 35.5 cm with 90 bend in middle
Dipole	50		(wires 0.4mm diameter x 20) 1λ separation at 22 GHz.
Wave plate	10	10	(wires 0.5mm diameter x 74) 1mm separation between plate and wires.
Wax block			3.8 cm thick, xx cm diameter.

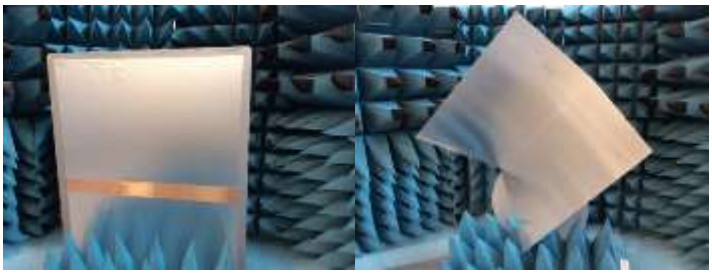

Figure 3. Flat plate reflector (left), Dihedral reflector angled at 45° (right).

Figure 4. Vertical dipole (left), Horizontal dipole (right)

The flat plate (left) and a dihedral reflector orientated at 45° (right) can be seen in Figure 3. Both of these targets are used in the calibration process previously described. An array of thin wires referred to as dipoles vertical (left), horizontal (right) can be seen in Figure 4. The theoretical response for these targets can be seen in Figure 5 [12]. For the flat plate it can be seen that the cross polar nulls are located around the equator of the Poincaré sphere indicating that no conversion is taking place for the linear polarisation states. The co-polar nulls are located at the zenith and nadir indicating that conversion takes place for the circular polarisation states. The dihedral at 45° shows the cross polar nulls transiting around the zenith and nadir, indicating that no conversion is taking place for the circular polarisation states. The co-polar nulls are located at the vertical and horizontal linear polarisation points on the Poincaré sphere indicating that conversion is taking place for these polarisation states.

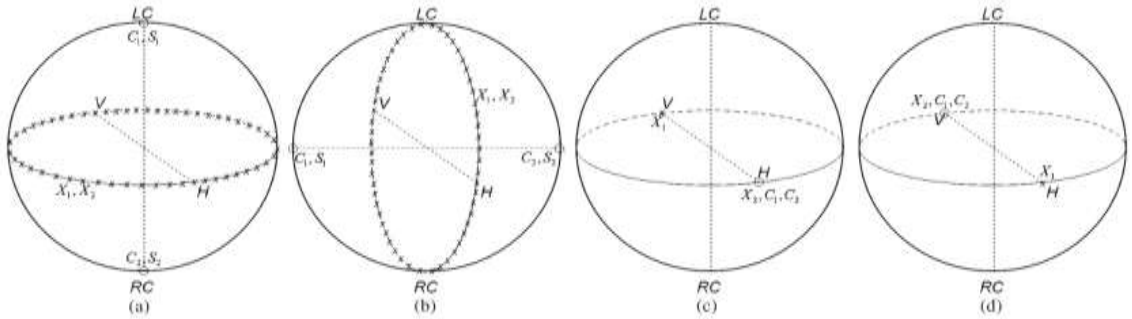

Figure 5 [12] (a) Flat plate, (b) Dihedral at 45°, (c) Vertical dipole, (d) Horizontal dipole.

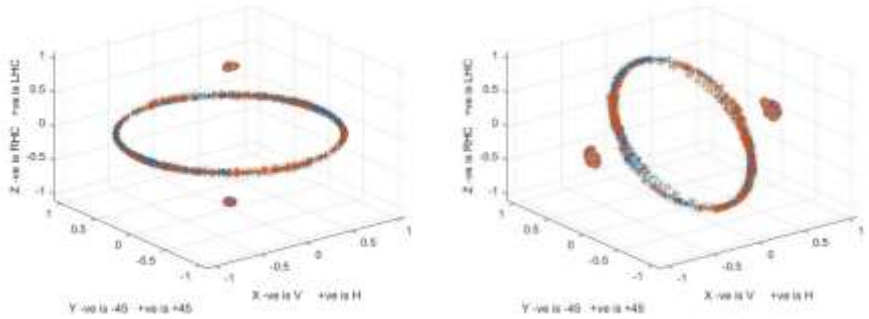

Figure 6. Measured responses, Flat plate (left), Dihedral 45° (right).

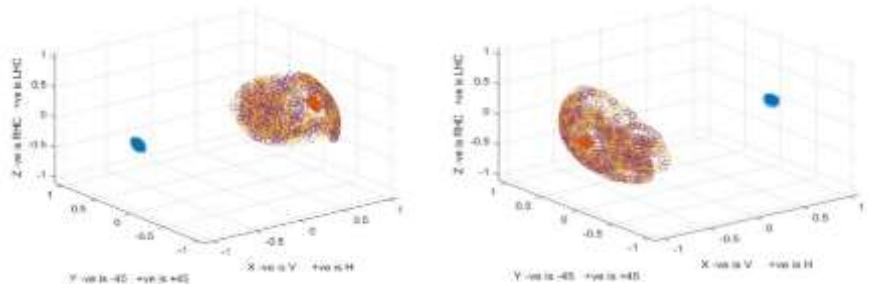

Figure 7. Measured responses, Long wires referred to as dipoles. Vertical dipole (left), Horizontal dipole (right).

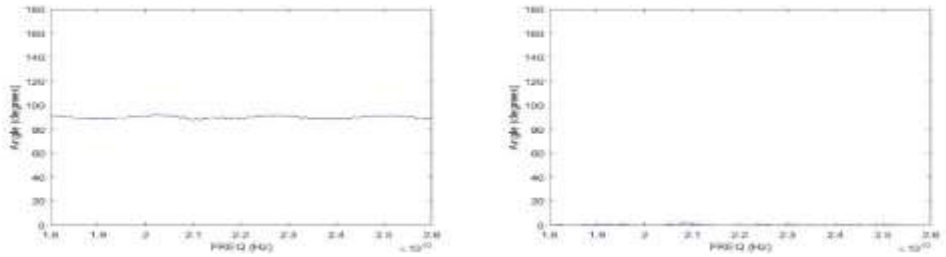

Figure 8. Huynen target Orientation angle (ϕ) for the dipole (vertical left horizontal right).

Figure 8 shows the Huynen target orientation angle for the dipole (vertical left, horizontal right), vertical being at 90° and horizontal at 0° calculated using Eq. 12. Figure 7 shows the measured dipole response showing a cone shaped distribution due to the target not being a perfect dipole.

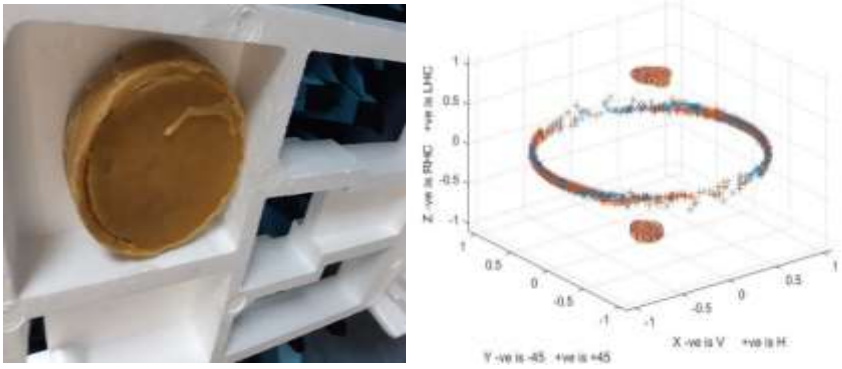

Figure 9. 3.8 cm thick wax block pictured left, measured results right.

Figure 9 (left) shows a 3.8 cm wax block with its measured response shown on the right. The measured response is identical to that for the flat plate previously shown however the Huynen polarization parameters contain further information about the target as will be seen next.

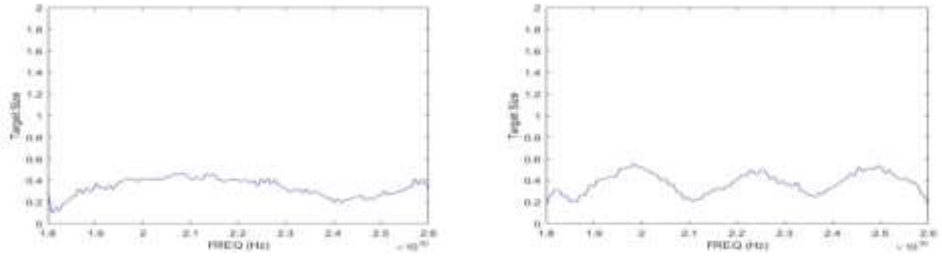

Figure 10. Huynen target size (m) (cavity fringes) Wax block 2cm thick (left), 3.8cm thick (right), refractive index n=1.47.

From Figure 10 of the Huynen target size (Eq. 19) for the wax block it will be noted a succession of peaks and troughs; the frequency difference between troughs on the right plot can be seen to be around 2.56 GHz. This frequency known as the fringe frequency spacing Δ_f is the result of constructive and destructive interference of waves internally reflected on this inside of the material. Equation 21 enables calculation of the fringe frequency spacing given the dielectric thickness, the refractive index and c is the speed of light. Assuming the block thickness to be unknown as in the case of a PBIED, but knowing the refractive index and measured fringe frequency then simple transposition enables determination of the dialectic thickness d. Assuming the dielectric constant for wax to be 1.47, and the measured fringe frequency for the thicker wax block to be 2.56 GHz then the dielectric thickness by calculation is 3.8cm which the block is in this case.

$$\Delta_f = \frac{c}{2.d.n} \tag{21}$$

6. CONCLUSION

Comparison with the measured results (Figure 6 for the flat plate and dihedral) and Figure 7 for the dipoles show good agreement with the theoretical responses [12], [17]. The Huynen target parameters reveal further target information that could be used for identification purposes. The examples presented show the orientation angle for a dipole with vertical and horizontal alignment. The Huynen polarisation parameter of target size enables the determination of dielectric thickness to be determined as in the case of a PBIED. In total seven pieces of target information are available.

7. FUTURE WORK

Future work will be carried out to determine if target motion causes depolarisation resulting in partial coherence. Movement of objects will be made and changes to the matrices will be noted and compared with theory. In the presence of depolarisation incoherent decomposition algorithms will be investigated which includes creating from the Sinclair matrices the coherency or covariance matrices. Measurements have shown that the Sinclair matrices change little between multiple measurements made of the same target when motion is not present. If depolarisation proves not to be an issue then further investigation in to the suitability of the Huynen polarisation fork approach as a means to identify targets will continue. A comparison with other coherent decomposition algorithms would also be of interest. If depolarisation does manifest itself due to target motion then application of the coherency or covariance matrix will be implemented. Whether or not the Huynen target parameters could still be determined in the presence of depolarisation remains to be seen. Future work will also be used in identifying the full polarimetric signatures of the human body alone, threat items alone, and when threats are concealed under clothing on the human body. In the case of the human body alone it may be useful to investigate the possibility that the skin of the human body has chirality in its response, which would be detected in the response to circular polarisation, as shown in [21]. Complete understanding of the signatures of the human body in the millimetre wave band are important for recognising anomalies for security screening purposes.

REFERENCES

[1] E. Blackhurst, N. Salmon and M. Southgate, “Full Polarimetric Millimetre Wave Radar for Stand-off Security Screening,” in *SPIE Security + Defence, 2017*, Warsaw, Poland, 2017.

[2] D. A. Andrews, N. Bowring, N. D. Rezgui, M. Southgate, E. Guest, S. Harmer and A. Atiah, "A multifaceted active swept millimeter wave approach to the detection of concealed weapons," *Proc. SPIE Millimetre Wave and Terahertz Sensors and Technology,* vol. 7117, 2008.

[3] D. A. Andrews, S. W. Harmer, N. J. Bowring, N. D. Rezgui and M. J. Southgate, "Active Millimeter Wave Sensor for Standoff Concealed Threat Detection," *IEEE SENSORS JOURNAL,* vol. 13, no. 12, 2013.

[4] D. A. Andrews, N. D. Rezgui, S. E. Smith, N. Bowring, M. Southgate and J. G. Baker, "Detection of concealed explosives at stand-off distances using wide band swept millimetre waves," in *Millimetre Wave and Terahertz Sensors and Technology*, Cardiff, 2008.

[5] S. W. Harmer, N. Bowring, D. Andrews, N. D. Rezgui, M. Southgate and S. Smith, "A Review of Nonimaging Stand-Off Concealed Threat Detection with Millimeter-Wave Radar," *IEEE Microwave magazine,* 2012.

[6] S. Hutchinson, *Investigation of late time response analysis for security applications,* Manchester: Manchester Metropolitan University, Manchester, UK, 2015.

[7] M. Southgate, *'Remote Detection of Concealed Guns and Expolosives', Phd dissertation,* Manchester: Manchester Metropolitan University, Manchester, UK, 2013.

[8] D. M. Sheen, D. L. McMakin, W. M. Lechelt and J. W. Griffin, "Circularly polarized millimeter-wave imaging for personnel screening," *Proc. SPIE 5789, Passive Millimeter-Wave Imaging Technology VIII, ; doi: 10.1117/12.606825,* 19 May 2005.

[9] D. O'Reilly, "A Feasibility Study On The Application Of Polarimetric Decomposition Algorithms To The Detection Of Concealed Weapons," Manchester Metropolitan University, Manchester, 2015.

[10] D. O'Reilly, N. Bowring, N. D. Rezgui and D. Andrews, "Target decomposition and polarimetric radar applied to concealed threat detection," *SPIE Millimetre Wave and Terahertz Sensors and Technology VI,* vol. 89000D, 2013.

[11] "ESA Earth Online," ESA, [Online]. Available: https://earth.esa.int/documents/653194/656796/Polarimetric_Decompositions.pdf. [Accessed 10th July 2018].

[12] A. Marino and S. Cloude, "A Polarimetric Target Detector Using the Huynen Fork," *IEEE Transactions on geocience and remote sensing,* vol. 48, no. 5, pp. 2357-2366, 2010.

[13] N. Alessandro and P. R. L., "A Turnstile Junction Waveguide Orthomode Transducer," *IEEE TRANSACTIONS ON MICROWAVE THEORY AND TECHNIQUES,* 2006.

[14] N. Alessandro, B. Alberto and P. R. L., "Test of 1 mm Band Turnstile Junction Waveguide Orthomode Transducer," in *17th International Symposium on Space Terahertz Technology*.

[15] F. T. U. Kamal Sarabandi, "Calibration of Polarimetric Radar Systems with Good Polarisation Isolation," *IEEE Transactions on Geoscience and Remote Sensing.,* vol. 28, no. 1, pp. 70-75, 1990.

[16] A. Xi and W. Boerner, "Determination of the characteristic polarization states of the radar target scattering matrix [S(AB)] for the coherent monostatic and reciprocal propagation space by using the complex polarisation ratio ρ transformation formulation," *Opt. Soc. Am. A,* vol. 9, no. 3, pp. 437-455, 1992.

[17] A. Agrawal and W. M. Boerner, "Redevelopment of Kennaugh's Target Characteristic Polarisation State Theory Using the Polarization Transformation Ratio Formalism for the Coherent Case," *IEEE Transactions on Geoscience and Remote Sensing,* vol. 27, no. 1, pp. 2-14, 1989.

[18] E. M. Kennaugh, *Effects of type and polarization on echo characteristics,* Columbus, Ohio: Antennas Laboratory, The Ohio State University, 1949-1954.

[19] J. Huynen, *Phenomenological theory of radar targets,* PhD dissertation, Drukkerij Bronder, Rotterdam, The Netherlands: Delft University of Technology, 1970.

[20] W. Boerner, W. Yan and A. Xi, "On the Basic Principles of Radar Polarimetry: Target Characteristic Polarisation State Theory of Kennaugh, Huynen's Polarization Fork Concept, and its Extension to the Partially Polarized Case," *Proceedings of the IEEE,* vol. 79, no. 10, pp. 1538-1550, 1991.

[21] I. Hayut, P. Ishai, A. Agranat and Y. and Felman, "Circular polarization induced by the three-dimensional chiral structure of human sweat ducts," *PHYSICAL REVIEW E,* vol. 89, no. 042715, 2014.